



euronoise

# Experimental and numerical investigation of the dynamics in spatial fluid-filled piping systems

Jan Herrmann, Thomas Haag, Stefan Engelke and Lothar Gaul

Institute of Applied and Experimental Mechanics, University of Stuttgart, Pfaffenwaldring 9, 70550 Stuttgart, Germany
herrmann@iam.uni-stuttgart.de

Hydraulic piping systems, such as fluid-filled break and fuel pipes in automotive applications, undergo strong acoustic excitation due to pressure pulsations of pump and valve operation. By fluid-structure coupling the sound transmission within the pipe may lead to a structural excitation of other car components causing excessive noise levels or even structural failure. In order to obtain a complete and reliable understanding of the wave propagation and vibration phenomena in spatial piping systems, a test rig is presented, consisting of a pressure source and a fluid-filled break pipe with an attached target structure. With this experimental setup, it is possible to quantify the acoustic sound transmission and to examine the dynamic behavior by transfer functions. The experimental results are compared with finite element simulations employing efficient model order reduction techniques for the fluid-structure coupled system. This research focuses on the identification of hydraulic resonances and the optimal mounting of the fluid-filled break pipe in order to minimize the structure-borne sound induced on the target structure.

# 1 Introduction

Fluid-filled piping systems in typical automotive applications encounter strong hydraulic excitation due to pump and valve operation. Strong fluid-structure interaction phenomena between the flexible pipe shell and the fluid partition are observed in spatial piping systems [1, 2]. The transition from fluid-borne sound to structure-borne sound induced on target structures such as the floor panel or other parts of the car body leads to undesired vibration and noise levels or even structural failure. This research examines wave propagation and vibration phenomena both in the fluid path and the structural path in order to develop techniques to minimize structure-borne sound induced on the target structure. The optimization of the mounting position of the piping assembly turns out to be a particularly efficient way to reduce structure-borne sound in a wide frequency range. The experiments are conducted using a reliable hydraulic test bench [3] in order to measure hydroacoustic and vibroacoustic transfer functions of a fluid-filled break pipe with an attached plate as target structure where the structure-borne sound is measured. The hydraulic excitation is realized with a dynamic pressure source. The experimental results are compared with finite element simulations of the fluid-structure coupled assembly. To avoid the harmonic analysis of the full complex spatial piping system, substructering and model order reduction techniques are applied. Due to the small component interfaces of automotive piping systems, the adaptation of the Craig-Bampton method [4, 5] to fluid-structure coupled piping systems as developed in [1, 6] is used as an efficient model order reduction strategy. Note that the mean flow velocity is negligible when compared with the hydroacoustic speed (Mach number $M << 1$) [1].

The present article is structured as follows: First, the hydraulic test bench and its instrumentation is explained and the finite element modeling including the used component mode synthesis (CMS) method is described. Hydraulic transfer functions resulting from the measurement and simulation are compared which reveals strong fluid-structure coupling. Then, the connection points of the pipe to the target structure (the so called clips) are varied and the optimal mounting position of the piping system is determined by comparing vibroacoustic transfer functions. The goal of this research is the optimization of the dynamics in automotive piping systems and to obtain a better understanding of fluid-structure interaction phenomena.

# 2 Experimental setup

The experimental setup of the hydraulic test bench is illustrated in Fig 1. The setup consists of a hydroacoustic pressure source and a hydraulic pipe with an attached target structure. The hydraulic pipe is a curved steel break pipe (lengths 0.7 + 0.3 m) filled with water. More details on the material and geometrical properties are given in Table 1 and 2. The mounting of the target structure is realized with two steel clips. The pressure source consists of two piezostacks which are arranged perpendicularly to the direction of wave propagation and on opposite sides of the hydraulic pipe. The piezostacks are driven by a power amplifier and a function generator and oscillate with opposite phase in order to excite pressure pulsations in the fluid column [3]. A sweep excitation is chosen in order to excite a wide frequency range. The repeated sweep signals have a cycle duration of 100 ms. A typical time signal of the inlet pressure $p_1$ and the corresponding FFT is depicted in Fig. 2. The housing of the pressure source is designed in such a way that most of the energy goes into the break pipe where the dynamic measurements are conducted. The supply pipe with the additional pump is required to fill and compress the fluid to ensure a stable fluid column without any air bubbles. The dynamic pressure pulsations are measured with piezoelectric pressure sensors, whereas the structure-borne sound on the target structure is measured with a tri-axial accelerometer. The used instrumentation captures both the fluid-

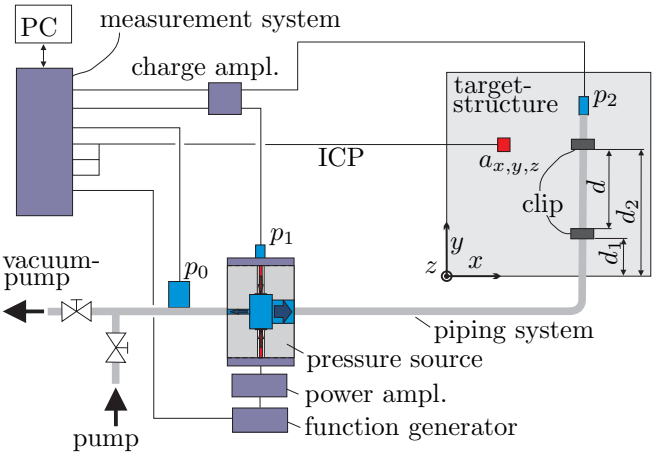


Figure 1: Experimental setup of the hydraulic test bench and definition of clip positions $d_1$, $d_2$ and clip distance $d$.

borne sound and the resulting structural excitation of the target structure and, in particular, flexural vibrations. The estimation of transfer functions is performed as explained in [7].

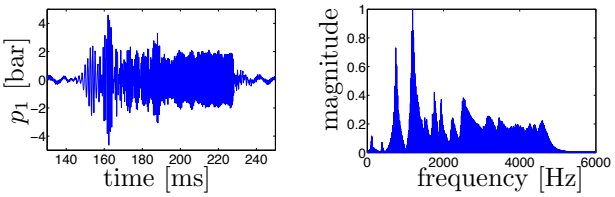


Figure 2: Typical time signal $p_1$ (left) and FFT (right).

| mat. | $E$ [GPa] | $\rho_s$ $[\frac{kg}{m^3}]$ | $\nu$ | $c_f$ $[\frac{m}{s}]$ | $\rho_f$ $[\frac{kg}{m^3}]$ |
|---|---|---|---|---|---|
| pipe | 206 | 7900 | 0.3 | – | – |
| plate | 180 | 7900 | 0.3 | – | – |
| clip | 210 | 7900 | 0.3 | – | – |
| fluid | – | – | – | 1460 | 1000 |

Table 1: Material properties.

| lengths | l x w x h [m] | $r_i$ [mm] | $r_o$ [mm] |
|---|---|---|---|
| pipe | – | 2.3 | 3 |
| plate | 0.3 x 0.3 x 0.001 | – | – |
| clip | 0.02 x 0.01 x 0.0225 | – | – |

Table 2: Geometrical properties.

## 3 FEM and model reduction

The substructures of the spatial piping assembly are modeled using the finite element method. The discretized fluid and structural partitions are coupled by a fluid-structure interface [8]. Two coupling conditions hold, namely the Euler equation

$$\rho_f \, \vec{n} \cdot \ddot{\vec{u}} = -\nabla p \cdot \vec{n} \tag{1}$$

with the displacements $\vec{u}$, the acoustic pressure $p$ and the normal direction $\vec{n}$, and the reaction force axiom

$$\vec{t} = -p\vec{n}, \tag{2}$$

here expressed in terms of Cauchy's stress vector $\vec{t}$ in the solid. The dynamic equations of the coupled finite element model are derived as described in [1, 8]

$$\underbrace{\begin{bmatrix} \mathbf{M}_s & \mathbf{0} \\ \rho_f \mathbf{C}^T & \mathbf{M}_f \end{bmatrix}}_{\mathbf{M}} \underbrace{\begin{bmatrix} \ddot{\mathbf{u}} \\ \ddot{\mathbf{p}} \end{bmatrix}}_{\ddot{\mathbf{x}}} + \underbrace{\begin{bmatrix} \mathbf{D}_s & \mathbf{0} \\ \mathbf{0} & \mathbf{D}_f \end{bmatrix}}_{\mathbf{D}} \underbrace{\begin{bmatrix} \dot{\mathbf{u}} \\ \dot{\mathbf{p}} \end{bmatrix}}_{\dot{\mathbf{x}}} + \underbrace{\begin{bmatrix} \mathbf{K}_s & -\mathbf{C} \\ \mathbf{0} & \mathbf{K}_f \end{bmatrix}}_{\mathbf{K}} \underbrace{\begin{bmatrix} \mathbf{u} \\ \mathbf{p} \end{bmatrix}}_{\mathbf{x}} = \begin{bmatrix} \mathbf{f}_s(t) \\ \mathbf{f}_f(t) \end{bmatrix} \tag{3}$$

with nodal displacements $\mathbf{u}$ and acoustic pressures $\mathbf{p}$. According to the Craig-Bampton method [4], a transformation with respect to the component interface degrees of freedom is followed by a model reduction in modal space. The reduction basis consists of constraint modes characterizing the static solution and fixed interface modes up to a certain frequency of interest as shown in [1]. The reduction basis $\mathbf{\Theta}_s$ of the solid domain and $\mathbf{\Theta}_f$ of the fluid domain are defined as

$$\begin{bmatrix} \mathbf{u}_I \\ \mathbf{u}_F \end{bmatrix} = \underbrace{\begin{bmatrix} \mathbf{I} \\ -\mathbf{K}_{s,FF}^{-1}\mathbf{K}_{s,FI} \end{bmatrix}}_{\substack{\text{constraint} \\ \text{modes}}} \underbrace{\begin{bmatrix} \mathbf{0} \\ \mathbf{T}_{s,FF} \end{bmatrix}}_{\substack{\text{fixed-interface} \\ \text{modes}}} \begin{bmatrix} \mathbf{u}_I \\ \mathbf{u}_d \end{bmatrix} = \mathbf{\Theta}_s \mathbf{q}_s, \tag{4}$$

$$\begin{bmatrix} \mathbf{p}_I \\ \mathbf{p}_F \end{bmatrix} = \underbrace{\begin{bmatrix} \mathbf{I} \\ -\mathbf{K}_{f,FF}^{-1}\mathbf{K}_{f,FI} \end{bmatrix}}_{\substack{\text{constraint} \\ \text{modes}}} \underbrace{\begin{bmatrix} \mathbf{0} \\ \mathbf{T}_{f,FF} \end{bmatrix}}_{\substack{\text{fixed-interface} \\ \text{modes}}} \begin{bmatrix} \mathbf{p}_I \\ \mathbf{p}_d \end{bmatrix} = \mathbf{\Theta}_f \mathbf{q}_f \tag{5}$$

with the generalized reduced coordinates $\mathbf{q}$. Note that index I indicates interface degrees of freedom (DOFs) and index F denotes free DOFs. The interface DOFs $\mathbf{u}_I$ and $\mathbf{p}_I$ are kept as physical DOFs which is typical for the applied Craig-Bampton method. The resulting reduction basis for the two-field problem is summarized as

$$\begin{bmatrix} \mathbf{u} \\ \mathbf{p} \end{bmatrix} = \begin{bmatrix} \mathbf{\Theta}_s & \mathbf{0} \\ \mathbf{0} & \mathbf{\Theta}_f \end{bmatrix} \begin{bmatrix} \mathbf{q}_s \\ \mathbf{q}_f \end{bmatrix}. \tag{6}$$

The reduced substructure contributions are assembled using the component mode synthesis (CMS) as described in [1, 4]. After the harmonic analysis of the reduced system, the results are expanded to full space in order to obtain the transfer function of interest. The finite element model of the assembled piping system with boundary conditions and a typical mode shape is depicted in Fig. 3. The assembly consists of 8 substructures, whereas a model order reduction up to a factor of 20 is achieved (67602 → 3370 DOFs). The three-dimensional modeling approach of the assembled piping system captures flexural vibrations of the pipe and target structure, which are particularly important in automotive applications.

## 4 Hydroacoustic transfer function

The measured and computed hydroacoustic (or hydraulic) transfer function $H_{p_1 \to p_2}$ is depicted in Fig. 4. The measured transfer function and correlation is estimated after measuring and averaging 30 swept pressure signals using the experimental setup as explained in section 2. The correlation between experiment and simulation is very good, both for the obtained hydraulic resonances and

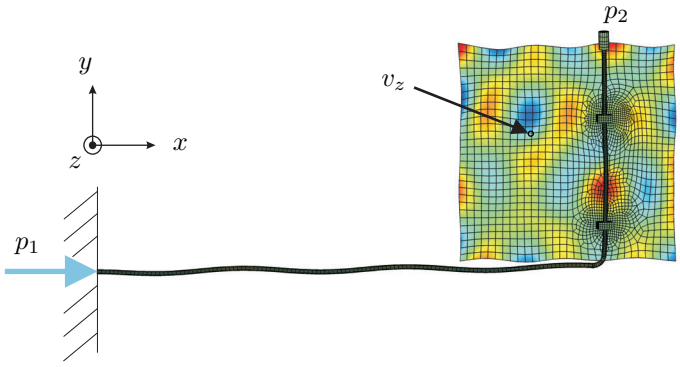


Figure 3: Finite element model of the assembled break piping system and boundary conditions; mode shape at $f$=1030 Hz (2nd hydraulic resonance).

the predicted damping in the fluid path. The frequency dependent fluid damping model is based on a complex wave number and accounts for wall friction effects [9], which are particularly important in slender pipes such as the present break pipe. A Rayleigh damping model is used to describe structural damping. Strong fluid-structure coupling is observed for a frequency around 1800 Hz, where the hydraulic and structural resonance coincides. Another fluid-structure coupled mode is visible around 3600 Hz. Note that the observed coupled modes are very sensitive with respect to the structural configuration and the pipe mounting position.

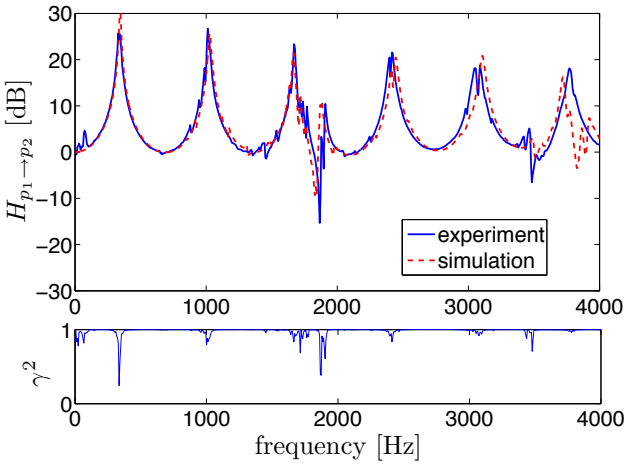


Figure 4: Hydraulic transfer function $H_{p_1 \to p_2}$ (top) and coherence of the measurement $\gamma^2$ (bottom).

# 5 Optimal mounting position of the piping system

Due to the pressure pulsations in the fluid and the strong fluid-structure coupling, the break pipe is excited and the structural vibrations are transferred by the clips to the target structure. To minimize the structure-borne sound induced on the target structure, the clip distance $d$, as defined in Fig. 1, is varied and the vibroacoustic transfer function between the input pressure $p_1$ and the normal velocity $v_z$ on a representative measurement point on the target structure is measured and computed. Section 5.1 summarizes the optimization scheme. In section 5.2, the evaluation of the vibroacoustic transfer function is described and the clip distance $d$ is varied in equidistant steps to compare the conducted measurements with simulation results. Here, the upper clip is fixed and the lower clip position $d_1$ is varied. Then, in section 5.3, both clip positions $d_1$ and $d_2$ (as defined in Fig. 1) are varied and the simulation is connected to an optimization algorithm to minimize the structure-borne sound on the target structure.

## 5.1 Optimization scheme

The substructure generation and CMS-procedure is automated in order to compute numerous piping assemblies to find the optimal mounting position of the break pipe. The optimization flow chart is shown in Fig. 5. The clip positions $d_1$ and $d_2$ as defined in Fig. 1, and thus the clip distance $d$ are varied and the ANSYS [10] input files of the relating substrucures (pipe sections, clip and target structure) are modified to achieve compatible meshes and to assemble the new piping system. After substructure generation, the system matrices and node/element tables are imported into Matlab [11], where the model reduction and the CMS-procedure is performed. The adjacent harmonic analysis of the reduced system is realized using modal superposition and the $\mathcal{H}_2$-Norm [12] of the vibroacoustic transfer function is computed which acts as objective function of the optimization. This calculation scheme is embedded into an optimization loop which minimizes the objective function. The used optimization algorithm is the Nelder-Mead simplex method [13, 14] (Matlab implementation: fminsearch).

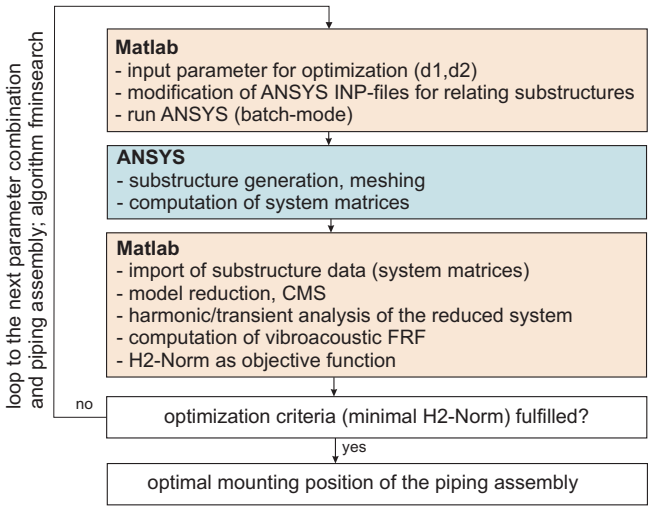


Figure 5: Optimization flow chart.

## 5.2 Evaluation of vibroacoustic transfer function

Since a wide frequency range with a high modal density of the relatively thin target structure is examined (up to 1500 Hz in the following), the $\mathcal{H}_2$-Norm is used as energy-based quadratic criterion [12] to evaluate the vibroacoustic transfer function $H_{p_1 \to v_z}$. The $\mathcal{H}_2$-Norm of

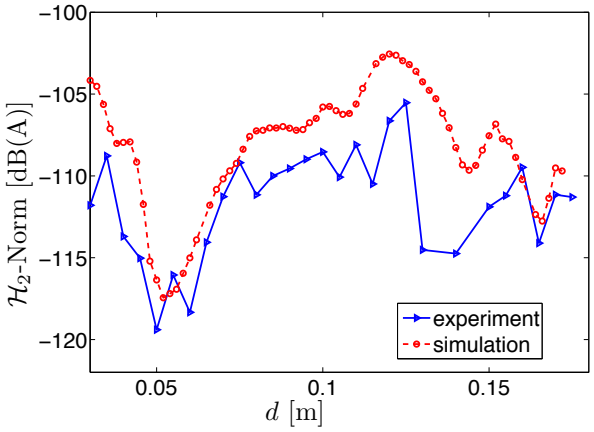


Figure 6: $\mathcal{H}_2$-Norm of the vibroacoustic transfer function $H_{p_1 \to v_z}$ as a function of clip distance $d$. Frequency range [0 1500] Hz.

a general transfer function $G(i\omega)$ is given as

$$\|G\|_2 = \sqrt{\frac{1}{2\pi} \int_{-\infty}^{\infty} \mathrm{tr}\left(G^*(i\omega) G(i\omega)\right) \, \mathrm{d}\omega}. \qquad (7)$$

The present study only considers Single-Input-Single-Output (SISO) systems and therefore the trace vanishes from Eq (7). Fig. 6 shows the $\mathcal{H}_2$-Norm of the vibroacoustic transfer function $H_{p_1 \to v_z}$ as a function of clip distance $d$ both for the measurement and simulation. Note that the upper clip is fixed and the lower clip position $d_1$ is varied in 2 mm-steps in the simulation and 5 mm-steps in the experiment. It is obvious from Fig 6 that, both for the measurement and the simulation, the optimal clip distance is around $d = 0.05$ m, whereas the unfavorable distance is around $d = 0.12$ m. So far, no optimization algorithm is used, but the clip distance is varied in equidistant steps. The measured vibroacoustic transfer function for the two border cases is depicted in Fig 7. It is obvious, that the pipe configuration with the unfavourable clip distance of $d = 0.12$ m leads to the largest structure-borne sound levels in the entire displayed frequency range. The piping assembly with the optimal clip distance is characterized by the alignment of the clips on nodal lines for dominant vibrations, and

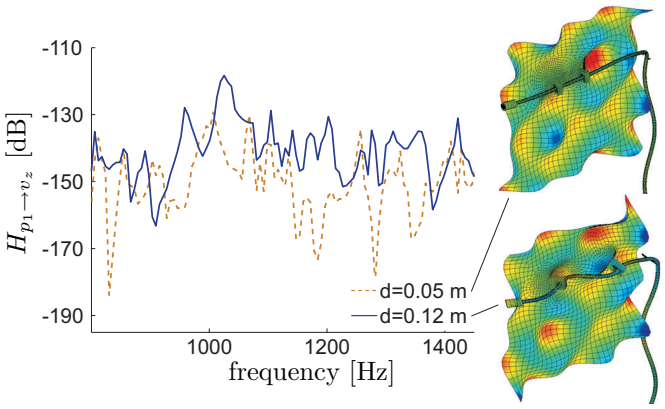


Figure 7: Measured vibroacoustic transfer function $H_{p_1 \to v_z}$ for the clip distances 0.05 m and 0.12 m and mode shape at f=1030 Hz.

hence, the induced structure-borne sound is minimized.

## 5.3 Optimization of mounting position

In the next step, the clip positions $d_1$ and $d_2$ are varied and the automatic substructuring and CMS-pocedure is coupled to the optimization algorithm as illustrated in Fig. 5. The relevant local minima are depicted in Fig. 8. For comparison, the result from the previous simulation of section 5.2, where only one parameter $d_1$ is varied, is shown in the same figure. The minimal value of the $\mathcal{H}_2$-Norm of the vibroacoustic transfer function $H_{p_1 \to v_z}$ is achieved for a clip distance of $d_{\mathrm{opt}} = 0.05739$ m (denoted as min2 in Fig. 8 and Table 3) after varying both clip positions $d_1$ and $d_2$. The optimization was successful after 43 iterations, whereas the $\mathcal{H}_2$-Norm was used as objective function with a termination tolerance of 0.001 dB. The initial values are $d_{1,0} = 0.094$ m, $d_{2,0} = 0.194$ m, and thus, $d_0 = 0.09$ m. More optimization data can be found in Table 3. The maximum function value of the $\mathcal{H}_2$-Norm is found for a clip distance of $d_{\mathrm{worst}} = 0.1199$ m. The difference between the optimized mounting position and the worst case scenario is $\mathcal{H}_{2,\mathrm{opt}} - \mathcal{H}_{2,\mathrm{worst}} = 17.44$ dB.

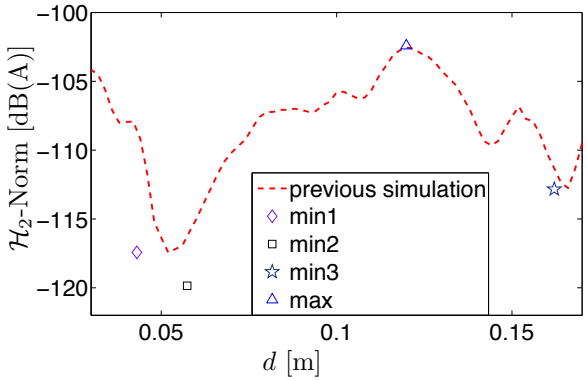


Figure 8: $\mathcal{H}_2$-Norm of the vibroacoustic transfer function $H_{p_1 \to v_z}$ as a function of clip distance $d$ (previous simulation) and optimization result after varying $d_1$ and $d_2$ (min1-min3 and max). Frequency range [0 1500] Hz.

| | iter. | $\mathcal{H}_{2,\mathrm{opt}}$ [dB(A)] | $d_{1,\mathrm{opt}}$ [m] | $d_{2,\mathrm{opt}}$ [m] |
|---|---|---|---|---|
| min1 | 28 | -117.43 | 0.1318 | 0.1848 |
| min2 | 43 | -119.86 | 0.0901 | 0.1575 |
| min3 | 26 | -112.84 | 0.0384 | 0.2105 |
| max | 25 | -102.41 | 0.0636 | 0.1935 |

Table 3: Optimization data: min1-min3 indicate local minima with the optimized parameter $d_{1,\mathrm{opt}}$ and $d_{2,\mathrm{opt}}$, max denotes the worst case.

# 6 Conclusion

Hydroacoustic and vibroacoustic transfer functions are measured with a hydraulic test bench and the results are confirmed by 3D finite element simulations including fluid-structure coupling and an efficient model order reduction strategy. A considerable noise and vibration reduction is achieved by geometric means such as the variation of the mounting position of the pipe. An optimization algorithm is implemented in the component mode synthesis procedure and the $\mathcal{H}_2$-Norm of the vibroacoustic transfer function is introduced as objective function. The optimization of the pipe mounting position leads to a considerable reduction (up to 17 dB) of the structure-borne sound induced on the target structure in a wide frequency range.

# 7 Acknowledgments

Funding of this project by the German Research Society DFG in the transfer unit TFB 51 "Simulation and Active Control of Hydroacoustics in Flexible Piping Systems" is gratefully acknowledged. Furthermore, the authors wish to thank Dr. Karl Bendel, Dr. Hans-Georg Horst and Dr. Berthold Käferstein at Robert Bosch GmbH for their help and advice.

# 8 References

# References

[1] M. Maess, "Methods for Efficient Acoustic-Structure Simulation of Piping Systems", Ph.D. thesis, Institute of Applied and Experimental Mechanics, University of Stuttgart, 2006.

[2] M. Maess, J. Herrmann, L. Gaul, "Finite element analysis of guided waves in fluid-filled corrugated pipes", *J. Acoust. Soc. Am.* **121**, 1313-1323 (2007).

[3] J. Herrmann, T. Haag, L. Gaul. K. Bendel, H.-G. Horst, "Experimentelle Untersuchung der Hydroakustik in Kfz-Leitungssystemen", In: *Proceedings of the 34th Deutsche Jahrestagung für Akustik DAGA*, Dresden, 2008.

[4] R.R. Craig, M.C.C. Bampton, "Coupling of substructures for dynamic analysis", *AIAA Journal* **6**, 1313-1319 (1968).

[5] R.R. Craig, A.J. Kurdila, *Fundamentals of Structural Dynamics*, John Wiley & Sons, Inc., New Jersey, 2006.

[6] M. Maess, L. Gaul, "Substructering and model reduction of pipe components interacting with acoustic fluids", *Mechanical Systems and Signal Processing* **20**, 45-64 (2006).

[7] D.J. Ewins, *Modal Testing: Theory, Practice, and Application*, Research Studies Press, 2003.

[8] O. Zienkiewicz, R. Taylor, *The Finite Element Method*, Butterworth-Heinemann, Oxford, 2000.

[9] H. Theissen, "Die Berücksichtigung instationärer Rohrströmung bei der Simulation hydraulischer Anlagen", Ph.D. thesis, RWTH Aachen, 1983.

[10] ANSYS Inc., *ANSYS Academic Research, Release 11*, 2007.

[11] The MathWorks, *MATLAB Release 7.4*, 2007.

[12] W. Gawronski, *Dynamics and Control of Structures*, Springer, New York, 1998.

[13] J.A. Nelder, R. Mead, "A simplex method for function minimization", *Computer Journal* **7**, 308-313 (1965).

[14] J.C. Lafarias, J.A. Reeds, M.H. Wright, P.E. Wright, "Convergence Properties of the Nelder-Mead Simplex Method in Low Dimensions", *SIAM Journal of Optimization* **9**, 112-147 (1998).